Proceedings World Geothermal Congress 2015
Melbourne, Australia, 19-25 April 2015

Development of Measuring Instruments for Fluid Flow Electromagnetic Method to Monitor Geothermal Fluid Flow

Toshiaki Tanaka and Hideki Mizunaga

Kyushu University, Motooka 744, Nishi-ku, Fukuoka 819-0395, Japan

tanaka@mine.kyushu-u.ac.jp

Keywords: Geothermal fluid flow, Monitoring, Instrument

ABSTRACT

Fluid Flow Electromagnetic Method is being developed for monitoring geothermal fluid flow behavior. The method can be applied to evaluate geothermal fluid distribution with time by measuring electromagnetic field distributions at each measurement node around the survey area. Measured values are transmitted periodically through wireless sensor networks from each measurement node to the survey base. Measurement nodes should be low-cost to reduce total survey cost, because a lot of measurement nodes are necessary to cover the survey area. Furthermore, it should also be low-power to reduce electric power consumption to be able to perform a long-term monitoring. Resulting from transmission experiments, dense arrangement of measurement nodes is required to reliably transmit measured values to the survey base through wireless sensor networks in vegetation environment.

1. INTRODUCTION

In order to evaluate the transient and dynamic behavior of subsurface fluid flow, such as geothermal fluid and ground water, a new geoelectrical technique named Fluid Flow Electromagnetic method is being developed (Mizunaga and Tanaka, 2010). The method is applied to visualize the dynamic behavior of fluid flow of fluid resources in reservoirs.

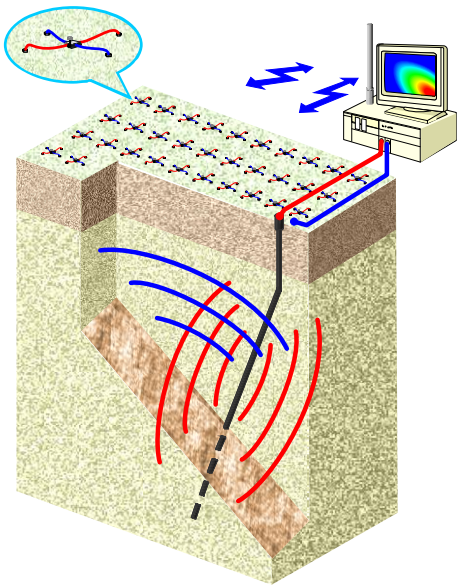

Figure 1: Schematic diagram of measurement system for Fluid Flow Electromagnetic method.

Figure 1 illustrates the concept of the measurement system for the Fluid Flow Electromagnetic (FFEM) method. The method is improved method hybridized the mise-á-la-masse method to evaluate resistivity distribution with the SP method to evaluate fluid flow distribution. Electromagnetic field changes caused by subsurface fluid flow behavior are measured at measurement nodes on the ground surface covering over the survey area. Electromagnetic anomalies are analyzed to evaluate fluid flow behavior.

2. ELECTROMAGNETIC PHENOMENA

A streaming potential associated with the fluid flow is known as an electrokinetic phenomena that occurs at the solid-liquid interface between matrix and water in porous media. A streaming electric current is a coupled electric current associated with fluid flow.

Considering the streaming potential mechanism, general equations for coupled flows for fluid flow and electric current can be written as follows(Fitterman, 1979; Sill, 1983; Ishido et al., 1983),

$$\mathbf{J} = -L_{11}\nabla P - L_{12}\nabla\Phi \quad (1)$$

$$\mathbf{I} = -L_{21}\nabla P - L_{22}\nabla\Phi \quad (2)$$

where **J** is the fluid flux **I** the current density, P the fluid pressure, Φ the electric potential, and L_{ij} the generalized conductivity. The Onsanger reciprocal relation requires that $L_{ij}=L_{ji}$.

When the effects of the secondary electric potentials on the fluid flow are small, the fluid flow equation is decoupled and resulting equations are

$$\mathbf{J} = -\frac{k}{\eta}\nabla P \tag{3}$$

$$\mathbf{I} = -C\nabla P - \sigma\nabla\Phi \tag{4}$$

where k is the hydraulic permeability, η the viscosity, σ the electric conductivity, C the cross-coupling coefficient defined as

$$C = -\frac{\varepsilon\zeta}{\eta} \tag{5}$$

where ε is the dielectric constant and ζ is zeta potential.

In the absence of current sources, $\nabla \cdot \mathbf{I}=0$,

$$\nabla\cdot(\sigma\nabla\Phi) = -\left\{\nabla\left(\frac{\varepsilon\zeta}{k}\right)\cdot\mathbf{J} + \frac{\varepsilon\zeta}{k}\nabla\cdot\mathbf{J}\right\} \tag{6}$$

Thus there are sources of conduction current wherever there are gradients of the cross-coupling coefficient parallel to the fluid flow or wherever there are fluid sources or sinks.

Magnetic fields due to electric currents can be described by the Biot-Savart law. An element of magnetic field is described by following relation.

$$dH = \frac{Idl\times r}{4\pi|r|^3} \tag{7}$$

where d**H**, I, d**l**, **r** are element of magnetic field vector, electric current, unit direction vector of electric current, position displacement vector from electric current element, respectively. Total magnetic field can be calculated as space integration of the magnetic field element (7).

3. DEVELOPMENT OF MEASUREMENT NODES

Simultaneous and continuous measurement of electromagnetic field caused by fluid flow behavior at measurement points on the ground surface is necessary to carry out Fluid Flow Electromagnetic (FFEM) survey.

Compact measurement nodes shown in Figure 2 for the survey are being developed. They can measure two components of electric field and three components of magnetic fields by internal high precision sensor circuits.

Figure 2: Measurement node and its inside.

The compact measurement node can be used for telemetry measurement in many points covering over the survey area with many measurement nodes. Because a lot of measurement nodes are necessary to cover the survey area, the measurement node should primarily be considered to be low-cost to reduce total survey cost in the development. Furthermore, it should also be low-power to reduce electric power consumption to be able to perform a long-term monitoring with small batteries.

3.1 Tilt and Azimuth Compensation

The measurement node has three kinds of different sensors, such as a tri-axial acceleration sensor, a tri-axial magnetic compass, and a high precision tri-axial magnetic sensor.

The tri-axial acceleration sensor is used to determine the tilt angle of the node by measured three components of gravitational accelerations. The tri-axial magnetic compass is used to determine the azimuth of the node. The high precision tri-axial magnetic sensor is used to measure the three components of the geomagnetic field variations generated by a streaming current caused by fluid flow behavior.

Measured components of the magnetic field variation in an arbitrary azimuth and tilt can be compensated by the combination of the tilt angle measured by the tri-axial acceleration sensor and the azimuth angle from the magnetic north pole measured by the tri-axial magnetic compass. As a result, the measurement node with the high precision tri-axial magnetic sensor can be installed on a ground surface in an arbitrary azimuth and tilt.

Some sensor manuals and data sheets of sensors (Grygorenko(2011), Ozyagcilar(2012), STMicroelectronics(2010)) describe tilt compensation algorithm with magnetic and acceleration sensors. For instance, the application note AN3192 provided by STMicroelectronics (2010) describes a tilt compensated electronic compass system.

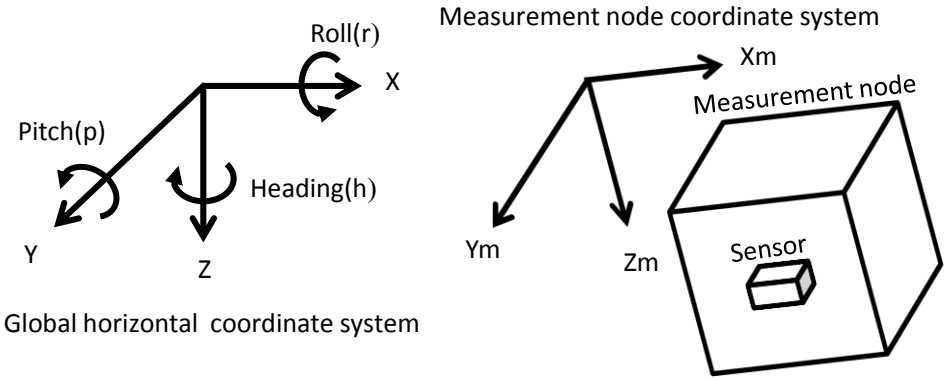

Figure 3: Global horizontal coordinate system heading to the magnetic north pole and local measurement node coordinate system.

X, Y, and Z are axes in the global horizontal coordinate system with heading to the magnetic north in a right-handed system.

Common representation for orientation rotating angles such as heading (h), pitch (p) , and roll (r) angles are defined as the rotating angle around the Z, X, and Y axes respectively.

When the measurement node is installed on a ground surface in an arbitrary azimuth and tilt, measured three components of the geomagnetic field variation need to be compensated.

Xm, Ym, and Zm are axes in a measurement node coordinate system as a local coordinate system.

The rotating matrix **Rh**, **Rp**, and **Rr** around Z, Y, and X axes respectively are

$$\mathbf{Rh}(h)=\begin{bmatrix}\cos(h) & \sin(h) & 0\\ -\sin(h) & \cos(h) & 0\\ 0 & 0 & 1\end{bmatrix} \tag{8}$$

$$\mathbf{Rp}(p)=\begin{bmatrix}\cos(p) & 0 & -\sin(p)\\ 0 & 1 & 0\\ \sin(p) & 0 & \cos(p)\end{bmatrix} \tag{9}$$

$$\mathbf{Rr}(r)=\begin{bmatrix}1 & 0 & 0\\ 0 & \cos(r) & \sin(r)\\ 0 & -\sin(r) & \cos(r)\end{bmatrix} \tag{10}$$

Different rotation procedures result in different rotation matrix.

The rotation matrix **R** after the three rotations **Rh** then **Rp** and finally **Rr** is represented as:

$$\begin{aligned}\mathbf{R}(r,p,h)&=\mathbf{Rr}(r)\cdot\mathbf{Rp}(p)\cdot\mathbf{Rh}(h)\\ &=\begin{bmatrix}\cos(p)\cos(h) & \cos(p)\sin(h) & -\sin(p)\\ \cos(h)\sin(p)\sin(r)-\cos(r)\sin(h) & \cos(r)\cos(h)+\sin(p)\sin(r)\sin(h) & \cos(p)\sin(r)\\ \cos(h)\sin(p)\cos(r)+\sin(r)\sin(h) & -\sin(r)\cos(h)+\sin(p)\cos(r)\sin(h) & \cos(p)\cos(r)\end{bmatrix}\end{aligned} \tag{11}$$

The unit vector **eg** (0,0,1) parallel to the gravitational vector in the global coordinate system is rotated by the rotation matrix **R** to make the unit vector **egm** (ex, ey, ez) parallel to the gravitational vector in the measurement node coordinate system.

The unit vector **egm** is represented by the measured acceleration vector **A** (Ax, Ay, Az) as:

$$\mathbf{egm} = \frac{\mathbf{A}}{|\mathbf{A}|} = \mathbf{R}(r, p, h) \cdot \mathbf{eg}$$

$$\frac{1}{\sqrt{A_x^2 + A_y^2 + A_z^2}} \begin{bmatrix} A_x \\ A_y \\ A_z \end{bmatrix} = \begin{bmatrix} \cos(p)\cos(h) & \cos(p)\sin(h) & -\sin(p) \\ \cos(h)\sin(p)\sin(r) - \cos(r)\sin(h) & \cos(r)\cos(h) + \sin(p)\sin(r)\sin(h) & \cos(p)\sin(r) \\ \cos(h)\sin(p)\cos(r) + \sin(r)\sin(h) & -\sin(r)\cos(h) + \sin(p)\cos(r)\sin(h) & \cos(p)\cos(r) \end{bmatrix} \begin{bmatrix} 0 \\ 0 \\ 1 \end{bmatrix} \tag{12}$$

Therefore, pitch (p) and roll (r) angle can be calculated by using measured accelerations as:

$$p = \sin^{-1}\left(\frac{-A_x}{|\mathbf{A}|}\right) \tag{13}$$

$$r = \sin^{-1}\left(\frac{A_y}{|\mathbf{A}|\cos(r)}\right) \tag{14}$$

For the heading angle calculation, tri-axial magnetic compass measurements need to be reflected onto the horizontal plane by tilt compensation.

The measurement node rotates from the global horizontal coordinate system to the measurement node coordinate system by roll angle rotation followed by pitch angle rotation.

Tilt compensated magnetic sensor measurements Mx, My, and Mz can be obtained from magnetic sensor raw measurements Mmx, Mmy, and Mmz as:

$$\begin{bmatrix} M_x \\ M_y \\ M_z \end{bmatrix} = R_r^{-1} R_p^{-1} \begin{bmatrix} M_{mx} \\ M_{my} \\ M_{mz} \end{bmatrix} = \begin{bmatrix} \cos(p) & 0 & \sin(p) \\ \sin(r)\sin(p) & \cos(r) & -\sin(r)\cos(p) \\ -\cos(r)\sin(p) & \sin(r) & \cos(r)\cos(p) \end{bmatrix} \cdot \begin{bmatrix} M_{mx} \\ M_{my} \\ M_{mz} \end{bmatrix} \tag{15}$$

Therefore, heading (h) angle can be calculated by using measured magnetic measurements as:

$$h = \begin{cases} \tan^{-1}\left(\frac{M_y}{M_x}\right) & for\ M_x > 0\ and\ M_y \geq 0 \\ 90° & for\ M_x = 0\ and\ M_y < 0 \\ 180° + \tan^{-1}\left(\frac{M_y}{M_x}\right) & for\ M_x < 0 \\ 270° & for\ M_x = 0\ and\ M_y > 0 \\ 360° + \tan^{-1}\left(\frac{M_y}{M_x}\right) & for\ M_x > 0\ and\ M_y \leq 0 \end{cases} \tag{16}$$

3.2 Measurement of Geomagnetic Field Variation

In order to carry out simultaneous measurement of electromagnetic field components for the FFEM survey, a small magnetic sensor with high sensitivity and low power consumption is required. Although both induction coils used for MT (Magnetotelluric) method and fluxgate magnetometers used for magnetic and electromagnetic methods are usually considered for magnetic field sensors, they are not suitable for the simultaneous measurement at the many measurement points for the FFEM survey because of their large size, heavy weight, and high cost.

MI (Magneto-Impedance) magnetic sensors shown in Figure 3 are suitable for the measurement of the magnetic field components for the FFEM survey. The MI sensor based on the magneto-impedance effect in amorphous wires is a very sensitive magnetic sensor having detection sensitivity equivalent to the fluxgate magnetic sensors (Mohri et al., 2002). The sensor has flat frequency response characteristics from DC to about 1MHz frequency band. Its power consumption is lower and its sensor size is smaller enough than fluxgate magnetic sensors.

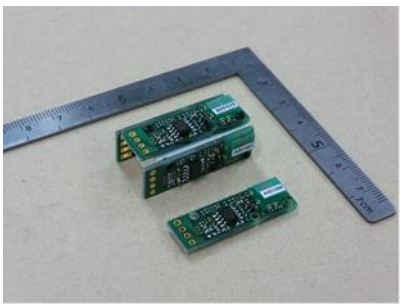

Figure 3: High precision MI(Magneto-Impedance) magnetic sensors.

3.3 Control Circuit

Recently, various semiconductors and sensors are developed for portable digital terminals and mobile phones. In order to realize low-cost, low-power consumption, and high-performance measurement system for the FFEM survey, latest semiconductor devices such as PSoC device are effectively applied to develop measurement nodes. PSoC developed by Cypress Semiconductor is a programmable embedded System-on-Chip device integrating configurable analog and digital circuits, memory, flexible input and output interfaces, and a microprocessor on a single chip. Minimal external components, devices and sensors can be used with PSoC to develop measurement nodes for the FFEM survey.

Configurable analog and digital circuits in the PSoC device are capable of adjusting gains of amplifiers and appropriate filter characteristics of noise filters for sensing circuits connecting some sensors. Especially, noise filters having appropriate frequency characteristics suitable for electric noise reduction around a survey area can be dynamically provided by itself with the PSoC devices after measuring raw signals containing electric noise before starting of measurements.

3.4 Wireless Sensor Network

The measurement node should be low-cost to reduce total survey cost, because a lot of measurement nodes are necessary to cover widely the survey area. Furthermore, it should also be low-power to reduce electric power consumption to be able to perform a long-term monitoring with small batteries. Measured values of the electric field and the magnetic field at measurement nodes are transmitted periodically by wireless connection from each measurement node to the survey base through the wireless sensor network (Figure 4) based on ZigBee technologies without wiring cables around a survey area.

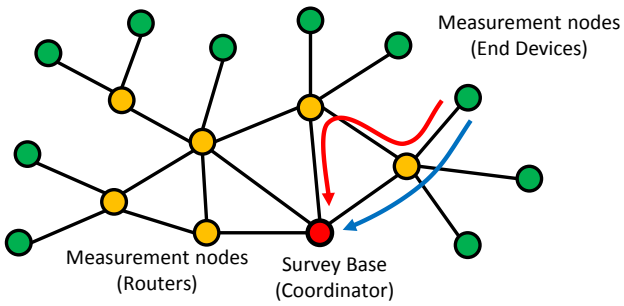

Figure 4. Configuration of wireless sensor networks connected with each measurement node and survey base.

ZigBee is a wireless technology developed as an open global standard to implement low-cost and low-power wireless M2M (machine to machine) networks. ZigBee networks are composed of three types of devices, such as Coordinators, Routers, and End Devices. There is only one Coordinator in one ZigBee wireless network. It can establish the network and control the network configuration and the security of the network. Routers relay information from devices to others as intermediate nodes. End Devices are sensor nodes at the end of the sensor networks. It cannot relay information to other devices but transmit measured values to Routers or the Coordinator. It should be low-power consumption and can shift to the sleep mode in which power consumption is suppressed.

Measurement nodes equipped with ZigBee modules and sensors in dense arrangement can configure wireless sensor networks covered over FFEM survey area. Measurement nodes can interconnect with adjacent measurement nodes to establish a plurality of transmission paths to the survey base. For example the red and the blue arrows via different Routers are deferent transmission paths from the one End Device in Figure 4.

Plural measured values are temporarily recorded every fixed period in the flash memory in the measurement node and periodically intermittently transmitted to the survey base through the wireless sensor network.

ZigBee networks can be installed easily to configure mesh networking. Its flexibility allows networks to be easily adapted to changing network configuration and range by adding, moving or removing nodes dynamically to follow electromagnetic anomalies around FFEM survey area during the long-term monitoring.

4. FIELD EXPERIMENT TO TRANSMISSION THROUGH VEGETASION ENVIRONMENT

ZigBee uses the frequency band of 2.4GHz for transmission. The transmission range may be more than 1km in free space with ideal conditions. High frequency radio wave propagation characteristics have high directivity.

Topographic features like ridges of mountains, standing trees and their leaves in vegetation environment may be obstacles to transmit measured values from measurement nodes to a survey base.

Because propagation characteristics of high frequency radio waves have high directivity, the transmission range in survey areas, in many geothermal areas, in vegetation environment or mountain areas may become shorter than that of in ideal free space by obstacles such as ridges of mountains, standing trees and bushes, located between measurement nodes.

In order to determine the effects of vegetation including standing trees and their leaves on the attenuation of the received signal strength according to the transmission distance of ZigBee modules considering FFEM surveys in vegetation environment and mountain area, comparative field experiments were carried out along a road and in vegetation environment in the campus of the university.

TWE-Regular modules made by Tokyo Cosmos Electric Co., Ltd. in Japan were selected for ZigBee transmission modules in measurement nodes for the FFEM survey because of its low-power consumption.

Evaluation of the attenuation of high frequency radio waves through standing trees and their leaves becomes important issue to develop measurement nodes for the FFEM survey mainly conducted in vegetation environments and mountain area.

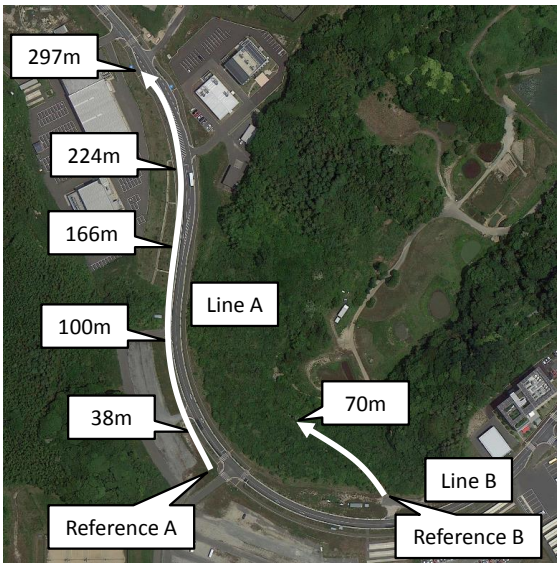

Figure 5. Field Experiments for transmission distance of ZigBee modules.

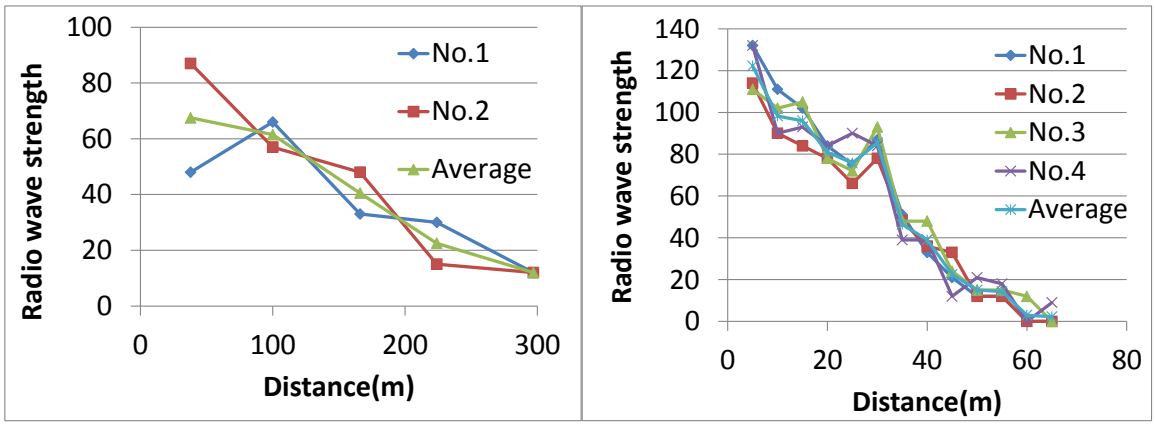

Figure 6. Radio wave signal strength distant from each reference in free space condition (left) and in vegetation environment (right).

For the transmission experiment in open space conditions shown in Figure 5, one Coordinator was placed at the reference point A on the side of the road with the height of 1.5m from the ground surface.

Two End Devices were placed together at the same measurement point with the height of 1.5m from the ground surface distant from the reference point along the road curved round slightly to the right and the left in line-of-sight with no obstacle between measurement points and the reference point A. The distance between measurement point on the Line A and the reference point A was increased gradually to 300m to measure the relationship between received signal strength and the transmission distance.

For another transmission experiment in vegetation environment, one Coordinator was placed with the height of 1.5m from the ground surface at the reference point B at the entrance of the path into the vegetation in the campus of the university. Four End Devices were placed together at the same measurement point on the Line B with the height of 1.5m from the ground surface at various distances up to 70m distant from the reference point B along the path.

Figure 6 shows that measured strength of transmission signals with small variation attenuated linearly to the distance between the Coordinator and End Devices.

In the experiments, the maximum transmission distance in free space conditions in this case is approximately 350m, while in vegetation environment approximately 50m.

Resulting from transmission experiments, attenuation of the high frequency radio waves for transmission signals between ZigBee modules to the distance is approximately 8 times larger in the vegetation environment than that in free space conditions because trees and their leaves can scatter and attenuate high frequency radio waves.

5. CONCLUSIONS

Measurement nodes for the Fluid Flow Electromagnetic method have been developed with latest semiconductor devices having low-cost, low-power consumption, and high precision features.

Measurement nodes can be installed on a ground surface in an arbitrary azimuth and tilt. Measured components of the magnetic field variation in an arbitrary azimuth and tilt angles can be compensated by the combination of the tilt angle measured by the tri-axial acceleration sensor and the azimuth measured by the tri-axial magnetic compass.

Measured values are temporarily recorded in the flash memory in measurement nodes and periodically intermittently transmitted to the survey base through the wireless sensor network connected with adjacent measurement nodes by ZigBee technologies.

To evaluate the relationship between the transmission distance and the attenuation of high frequency radio waves used with ZigBee modules in vegetation environments, comparative field experiments were carried out in open space condition and in vegetation environment.

Comparative experiments of transmission distance show that the maximum transmission distance in free space conditions in line-of-sight is approximately 350m, while in vegetation environment approximately 50m.

Therefore, Measurement nodes equipped with ZigBee modules in dense arrangement should configure wireless sensor networks covered over FFEM survey area in vegetation environment.

REFERENCES

H. Mizunaga and T. Tanaka, Imaging of Geothermal Fluid Flow by Using Fluid Flow Electromagnetic Method, *Proceedings* of World Geothermal Congress 2010, 2010.

D. V. Fitterman, Calculations of self-potential anomalies near vertical contacts, *GEOPHYSICS*, **44**, No.2, 1979, pp. 195-205.

W. R. Sill, Self-potential modeling from primary flows, *GEOPHYSICS*, **48**, 1983, pp. 76-86.

T. Ishido et al., Streaming potential observations, using geothermal wells and in situ electrokinetic coupling coefficients under high temperature, *TECTONOPHYSICS*, **91**, 1983, pp. 89-104.

T. Tanaka and H. Mizunaga, Development of the measurement system for the fluid flow electromagnetic method using a low-power wireless sensor network, *Proceedings* of the 128th SEGJ Conference, 2013, pp.239-241.

V. Grygorenko, Sensing – Magnetic Compass with Tilt Compensation, Cypress Semiconductor Application Notes, AN2272, 2011.

T. Ozyagcilar, Implementing a Tilt-Compensated eCompass using Accelerometer and Magnetometer Sensors, Freescale Semiconductor Application Note, AN4248, 2012.

STMicroelectronics, Using LSM303DLH for a tilt compensated electronic compass, STMicroelectronics Application note, AN3192, 2010.